Evaluation of diethylnitrosamine- or hepatitis B virus X gene-induced hepatocellular carcinoma with ^{18}F-FDG PET/CT: A preclinical study

JU HUI PARK[1,2], JOO HYUN KANG[1], YONG JIN LEE[1], KWANG IL KIM[1], TAE SUP LEE[1], KYEONG MIN KIM[1], JI AE PARK[1], YIN OHK KO[1], DAE-YEUL YU[3], SANG-SOEP NAHM[4], TAE JOO JEON[5], YOUNG-SEO PARK[2] and SANG MOO LIM[6]

[1]Molecular Imaging Research Center, Korea Institute of Radiological and Medical Sciences (KIRAMS), Seoul 139-706; [2]Department of Food Science and Biotechnology, Gachon University, Gyeonggi-do 461-701; [3]Animal Molecular Physiology Research Unit, Korea Research Institute of Bioscience and Biotechnology, Daejeon 305-806; [4]Department of Veterinary Medicine, College of Veterinary Medicine, Konkuk University, Seoul 143-701; [5]Department of Nuclear Medicine, Gangnam Severance Hospital, Seoul 135-720; [6]Department of Nuclear Medicine, KIRAMS, Seoul 139-706, Republic of Korea

Received June 25, 2014; Accepted October 7, 2014

DOI: 10.3892/or.2014.3575

Abstract. The aim of this study was to evaluate whether the development of hepatocellular carcinoma (HCC) in murine models resembles tumor progression in humans, using non-invasive molecular imaging methods. Murine HCC models were generated by treating mice with diethylnitrosamine (DEN) or by the transgenic expression of hepatitis B virus X (HBx) protein (HBx-Tg model). Tumor development was detected using ^{18}F-fluoro-2-deoxyglucose (^{18}F-FDG) positron emission tomography (PET)/computed tomography (CT) and magnetic resonance imaging (MRI). The histopathological changes and expression of glucose transporter 1 (Glut1) and hexokinase 2 (HK2) were evaluated using hematoxylin and eosin and immunohistochemical staining, respectively. Tumor lesions as small as 1 mm in diameter were detected by MRI. Tumor development was monitored using ^{18}F-FDG PET/CT at 6.5-10 months after DEN treatment or 11-20 months after birth of the HBx-Tg model mice. A correlation study between the ^{18}F-FDG uptake levels and expression levels of HK2 and Glut1 in developed HCC showed a high ^{18}F-FDG uptake in poorly differentiated HCCs that expressed high levels of HK2, in contrast to that in well-differentiated tumors. The progression of primary HCCs resembling human HCC in murine models was detected and monitored by ^{18}F-FDG PET/CT. The correlation between tumor size and SUV_{max} was verified in the two HCC models. To the best of our knowledge, this is the first study to demonstrate that *in vivo* ^{18}F-FDG uptake varies in HCCs according to differentiation grade in a preclinical study.

Correspondence to: Dr Joo Hyun Kang, Molecular Imaging Research Center, Korea Institute of Radiological and Medical Sciences (KIRAMS), 75 Nowon-gil, Gongneung-Dong, Nowon-Gu, Seoul 139-706, Republic of Korea
E-mail: kang2325@kirams.re.kr

Key words: diethylnitrosamine, hepatitis B virus X protein, hepatocellular carcinoma, ^{18}F-FDG-PET/CT, tumor grading

Introduction

Non-invasive imaging methods are indispensable for detecting and diagnosing tumors in internal organs, such as the liver and brain. Among various imaging modalities, computed tomography (CT) and magnetic resonance imaging (MRI) provide anatomical information, whereas positron emission tomography (PET) provides functional information regarding a disease. Since each imaging modality has unique advantages and disadvantages (1,2), appropriate complementary imaging technologies have been developed. PET is widely used in nuclear medicine for the diagnosis of diverse malignant tumors and monitoring tissue metabolism (3).

PET imaging is achieved by use of radiotracers, with ^{18}F-fluoro-2-deoxyglucose (^{18}F-FDG) being commonly used in clinical practice for evaluation of the metabolic status of abnormal and normal tissues (4). ^{18}F-FDG is actively transported into cells by the same transporters that incorporate glucose (5), and is then phosphorylated by hexokinase 2 (HK2) or glucokinase and converted to FDG 6-phosphate, which is trapped in the cell immediately after phosphorylation (5). Increased glucose uptake is characteristic of malignant tumors, because tumors have increased expression levels of glucose transporters and intracellular enzymes, such as HK2, that are involved in glycolysis (6).

The intracellular concentration of ^{18}F-FDG in tumors typically represents the glycolytic activity of viable tumor cells. However, the detection of primary hepatocellular carcinoma (HCC) is less successful because ^{18}F-FDG uptake varies among tumor cells at different stages of differentiation (7).

For example, the detection rate of HCCs by ^{18}F-FDG PET varied from 50 to 70% in findings of previous studies (8-10). However, ^{18}F-FDG PET has been effective in the detection of poorly differentiated HCC (10,11) and has been considered valuable for detecting extrahepatic metastasis and assessing the response to treatment after molecular-targeted therapy (11).

HCC is one of the most common human cancers and its incidence is on the increase worldwide according to epidemiological data (12). The precise molecular mechanism underlying HCC progression is poorly understood. Therefore, it is essential to establish an animal model of HCC to monitor tumor progression and the efficacy of therapeutic intervention. In this respect, a xenograft model using immune-deficient mice, such as athymic or severe combined immune deficiency mice, is benificial, such as being readily and rapidly established and that it can be used effectively and efficiently when the appropriate cell lines are selected (13). However, as is the case for any animal model, tumor progression and the tumor microenvironment may not precisely reflect the human counterpart (14). Therefore, new models that can precisely reflect the progression of malignancies in humans should be identified.

Genetically modified mouse models (GMM), as well as models based on treating mice with chemical carcinogens that mimic the pathophysiological and molecular features of HCC in humans are available (14). GMMs are generally produced by the transgenic expression of oncogenes, such as c-myc (15), H-Ras (16) and hepatitis B virus (HBV)-associated genes (17,18) under the control of tissue-specific promoters. Furthermore, several chemical carcinogens are known to induce HCC, including diethylnitrosamine (DEN) (19), aflatoxin (20), thioacetamide (21) and carbon tetrachloride (22).

Among the chemical carcinogens that can induce HCC, the carcinogenicity of DEN is due to alkylation of cellular DNA (23) and generation of reactive oxygen species (24). The mechanism of HCC development following the administration of a single dose of DEN depends on the dosage of DEN used and the gender and age of the mice (25). Thus, DEN induced HCC in 100% of male and in 30% of female mice. The gender disparity in HCC incidence was caused by MyD88-dependent production of interleukin-6 (26). In the present study, we utilized murine models that resemble HCC in humans, through transgenic mice expression of the oncogenic hepatitis B virus X (HBx) and DEN-treated mice. We then evaluated primary HCC and monitored HCC progression longitudinally using ^{18}F-FDG small animal PET/CT and 3-T clinical MRI and compared ^{18}F-FDG uptake at different stages of tumor differentiation.

Materials and methods

HCC tumor-bearing mouse models. The care, maintenance and treatment of animals in these studies followed protocols approved by the Institutional Animal Care and Use Committee of the Korea Institute of Radiological and Medical Sciences.

Female and male C57BL/6 mice were purchased from The Central Lab, Animal Inc., Seoul, Korea and transgenic mice expressing the HBx (HBx-Tg model) were provided by Yu *et al* (17). The mice were maintained at 22-24˚C and 45-60% relative humidity, and had free access to food and water, in an air-conditioned incubator. To establish the chemical carcinogen-induced hepatic tumor model (DEN-model), 3-week-old male mice were injected intraperitoneally once with DEN at 20 mg/kg body weight (Sigma Aldrich, St. Louis, MO, USA).

MRI. MRI scanning was performed using a clinical 3-T MR unit (Magnetom Tim Trio, Siemens Medical Solutions, Erlangen, Germany) with a wrist coil, and the mice were fixed in a prone position. Fourteen mice were scanned at 19-21 months after DEN treatment and 13 HBx-Tg mice were scanned at 11-19 months after birth. Prior to scanning, the animals were anesthetized with 2% isoflurane in oxygen. The imaging parameters for the T2-weighted volumetric interpolated brain examination sequence were: repetition time (TR) =1,620 msec, echo time (TE) =37 msec, 60-mm field of view (FOV), 256x256 matrix size, 1-mm slice thickness, and number of excitations =2. Tumor size was calculated by measuring the diameter from MRI using Piview software (Mediface, Korea).

Small animal PET/CT study. Mice harboring HCC, as detected with 3-T MRI, were fasted overnight prior to ^{18}F-FDG PET/CT scanning. The mice were anesthetized with 2% isoflurane in oxygen and injected into the tail vein with 7.4 MBq of ^{18}F-FDG and then kept in a chamber with 0.5% isoflurane for 1 h. PET/CT images were obtained using an Inveon small animal PET/SPECT/CT system (Siemens Medical Solutions). The CT scan was conducted, and then PET/CT images were obtained using the following settings: CT scan total rotation of 360˚, estimated scan time of 180 sec; X-ray exposure time of 300 msec, average frame of 1 and effective pixel size of 109.63 μm, with fluoroscopy scan time of 60 sec, X-ray voltage and current of 70 kVp and 400 μA, respectively. PET images were scanned using a 1,200 sec acquisition time and a 511-KeV energy level (lower level was 350 KeV and the upper level, 650 KeV). During acquisition of the PET images, the mice were anesthetized using 2% isoflurane.

^{18}F-FDG was obtained from the Korea Institute of Radiological and Medical Sciences. The level of ^{18}F-FDG uptake in tumor nodules was measured as max standard uptake values (SUV_{max}), in which uptake activity was normalized for body weight and injected activity. Reconstruction of data sets, PET-CT fusion and image analysis were performed using Inveon Research Workplace (IRW) software (Siemens Medical Solutions).

Histopathological evaluation and immunohistochemistry. To evaluate the histopathological changes of the induced tumors, mice were euthanized and the liver tissues containing visible cancer masses were dissected. The specimens were washed with cold phosphate-buffered saline, fixed in 10% neutral buffered formalin and then embedded in paraffin. The tissue blocks were cut into 5-μm sections and subjected to hematoxylin and eosin (H&E) staining for light microscopy. Tumor regions with high or low ^{18}F-FDG accumulations were dissected, removed and processed separately.

Immunohistochemistry (IHC) was performed to determine the level of HK2 (HK2 monoclonal antibody, Thermo Scientific, Waltham, MA, USA) and Glut1 (Glut1; anti-GLUT1 antibody, Abcam, Cambridge, UK). Tissue sections were deparaffinized, rehydrated and incubated with 3% hydrogen peroxide for 20 min to block the endogenous peroxidase activity. Blocking was performed with 10% goat serum for 10 min. The sections

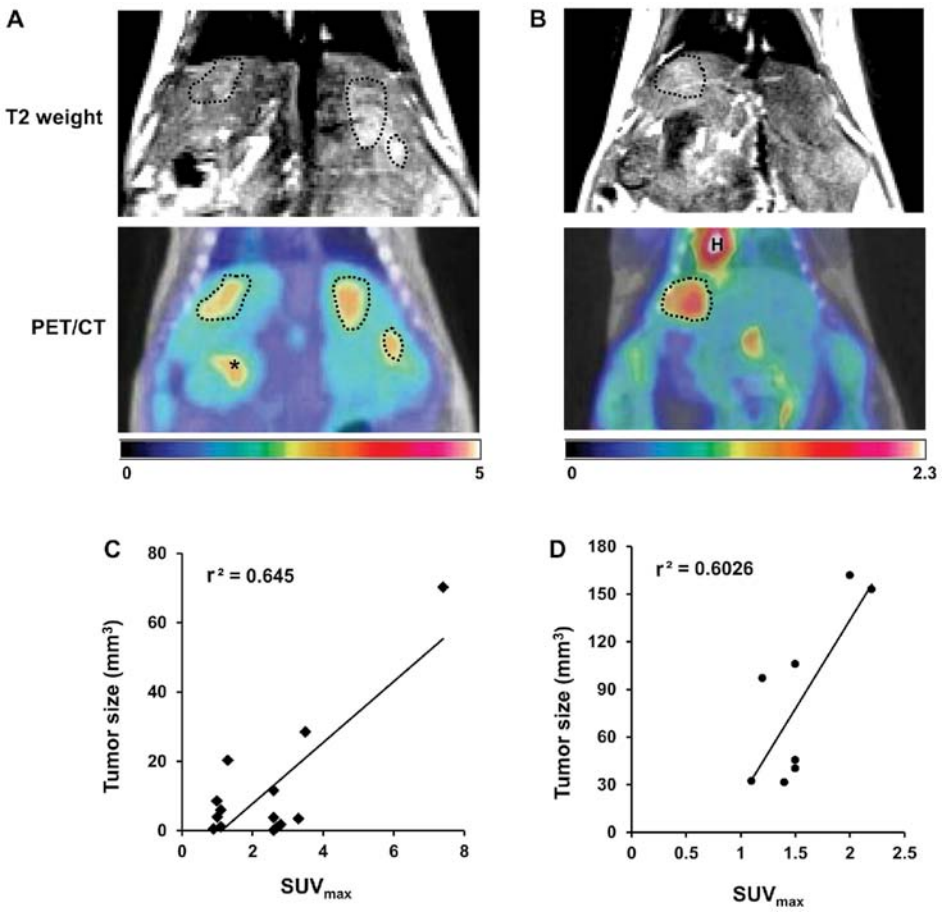

Figure 1. Representative T2-weighted magnetic resonance image (MRI) (upper panel) and ^{18}F-fluoro-2-deoxyglucose (^{18}F-FDG) PET/CT images (lower panel) at 19 months after treatment with (A) diethylnitrosamine (DEN) and of a (B) hepatitis B virus X protein (HBx-Tg model) at 11 months after birth. ^{18}F-FDG PET/CT images were obtained after MRI acquisition with a T2-weighted sequence. (C and D) Correlation of tumor size and SUV_{max} in the DEN and HBx-Tg models, respectively. Dotted line, H and asterisk indicate tumors, heart and stomach, respectively.

were incubated with primary antibody at 4˚C overnight and then with the appropriate secondary and tertiary antibodies for 30 min at room temperature. After washing, signals were detected using diaminobenzidine. Sections incubated without primary antibody served as negative controls. After examination of stained sections, the relative intensity of the immunoreactivity was classified into 3 grades: + (weak signal), ++ (medium signal) and +++ (fairly strong signal).

Results

Detection of induced HCC and multiple tumor lesions. The development of HCC in the DEN- or HBx-Tg model was observed using a clinical 3-T MRI capable of detecting tumors >1 mm in diameter. Lesions of this size were readily detected using MRI, but not with the small animal ^{18}F-FDG PET due to a resolution difference between the two imaging systems. Using MRI, tumors were detected in mice aged 6.5-21 months and 11-17 months in the DEN and HBx-Tg models, respectively.

The incidence of lesions was 50% (7/14 mice) in the DEN model and 38% (5/13 mice) in the HBx-Tg model. Eighteen and 11 multiple tumors developed in seven DEN- and five HBx-Tg model mice, respectively. Approximately 1-8 nodules of varying size were detected in each mouse. For example, three nodules induced by DEN throughout the liver (Fig. 1A) and one nodule by HBx oncogene (Fig. 1B) were visualized by MRI and ^{18}F-FDG PET/CT. There was a correlation between tumor size and SUV_{max} in the DEN-model (r^2=0.645) and HBx-Tg model (r^2=0.6026) (Fig. 1C and D, respectively).

Longitudinal monitoring of tumor growth using ^{18}F-FDG PET/CT. Tumor progression was monitored longitudinally and non-invasively using ^{18}F-FDG PET/CT. Tumors in DEN-model mice were first detected 6.5 months after DEN treatment and were longitudinally monitored until 10 months (Fig. 2A). In the HBx-Tg model mice, tumor nodules were observed at 11 months after birth and were followed up to 20 months (Fig. 2B). The increased size of tumor nodules was also assessed by the enhanced ^{18}F-FDG uptake in PET (Fig. 2).

Histopathological evaluation for verification of HCC. The sizes of the HCC nodules varied in the two models. The tumor nodules were either encapsulated by connective tissue or not well circumscribed (Fig. 3B and C). Following histopathological examination, tumor nodules were identified as either hepatocellular adenoma (HCA) or carcinoma. HCA was developed in the DEN- and HBx-Tg model mice and showed characteristics typical of adenoma, including irregular hepatic cord cells and vacuolated cytoplasm (arrows, Fig. 3B). HCC was also evident in the two models. In HCCs, the architecture

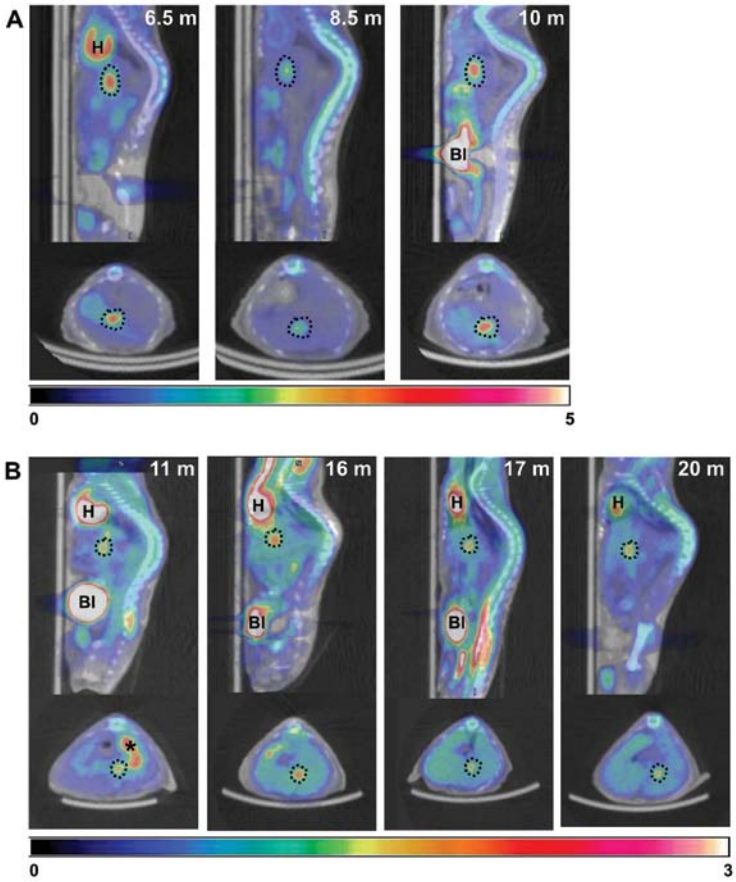

Figure 2. Monitoring of tumor progression in (A) diethylnitrosamine (DEN-model) and (B) hepatitis B virus X protein (HBx-Tg) model by ^{18}F-fluoro-2-deoxyglucose (^{18}F-FDG) PET/CT. Tumors were first detected in DEN-model mice at 6.5 months after DEN treatment and were longitudinally observed during hepatocarcinogenesis (at 8.5 and 10 months). HBx-Tg model mice were serially imaged after birth from 11 to 20 months. Dotted line, H, Bl and asterisk indicate tumors, heart, bladder and non-specific uptake lesion, respectively.

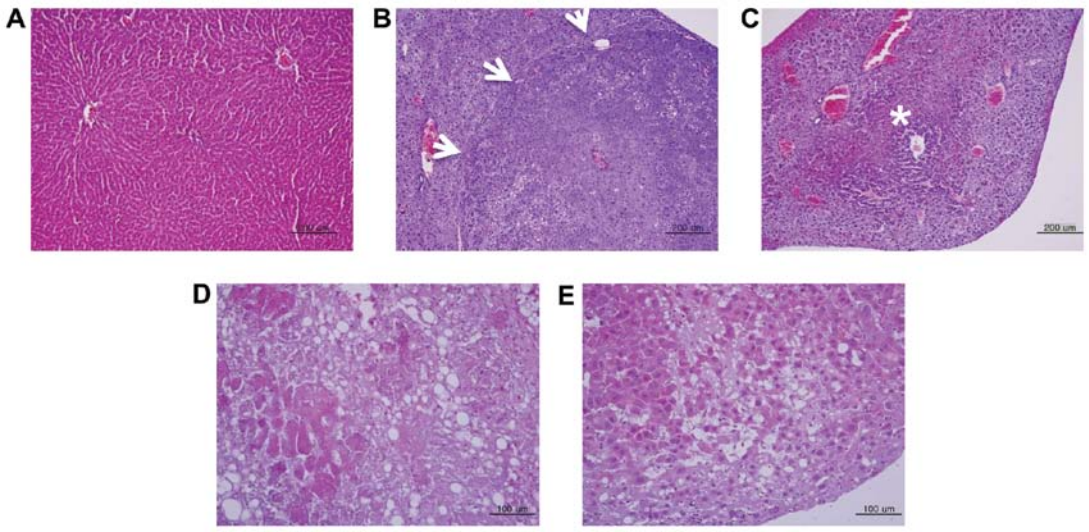

Figure 3. Representative photomicrographs of hematoxylin and eosin-stained tumor in the diethylnitrosamine (DEN) and hepatitis B virus X protein (HBx-Tg) model. A normal arrangement of hepatocytes is observed in the (A) control mouse liver, (B) hepatocelluar adenoma in DEN model and (C) carcinoma in the HBx-Tg model. Note that tumor nodules are either encapsulated (B, arrows) or diffuse (C, asterisk) within the liver tissue. Hepatocellular carcinoma (HCC) induced in the HBx-Tg model showed either (D) poorly differentiated carcinoma with high ^{18}F-fluoro-2-deoxyglucose (^{18}F-FDG) uptake or (E) well-differentiated carcinoma with low ^{18}F-FDG uptake.

of the hepatocytes appeared to be irregular and the tumor nodules contained pleomorphic cells (Fig. 3C-E). The cellular arrangement of HCC that developed in HBx-Tg mice was either that of a poorly differentiated (Fig. 3D) or well-differentiated carcinoma (Fig. 3E). We found that HCCs from high ^{18}F-FDG uptake tumor nodules were poorly differentiated, while one

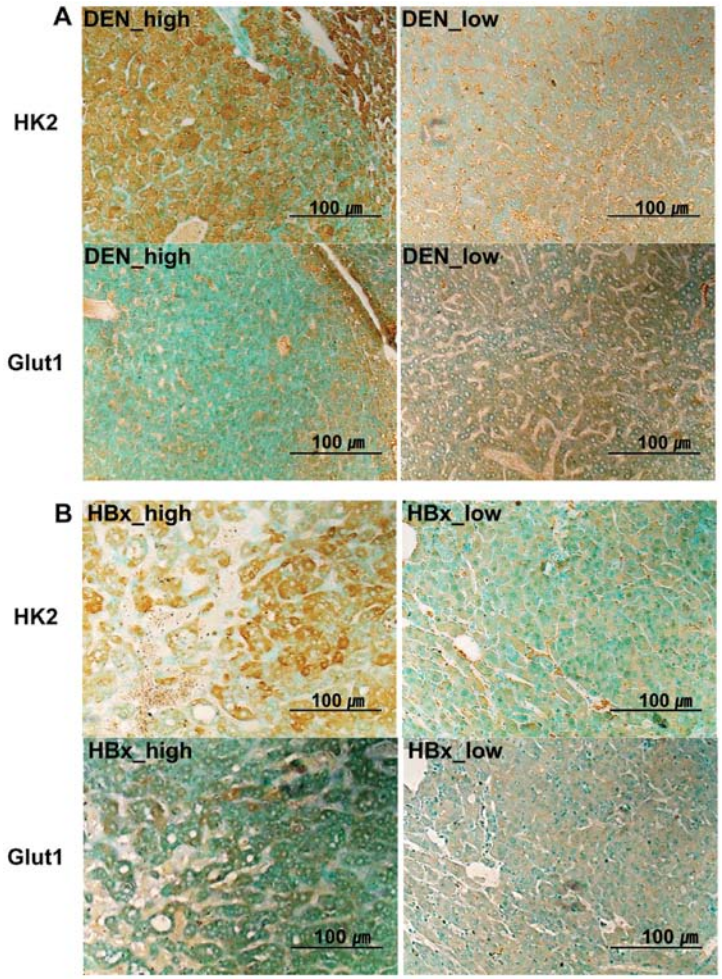

Figure 4. Representative photomicrographs of immunohistochemical staining for hexokinase 2 (HK2) and glucose transporter 1 (Glut1). A higher HK2 expression was observed in high ^{18}F-FDG uptake tumors compared with the low uptake tumor of ^{18}F-FDG in the (A) diethylnitrosamine (DEN model) and (B) hepatitis B virus X protein (HBx-Tg model). The levels of Glut1 expression did not differ in the high or low ^{18}F-fluoro-2-deoxyglucose (^{18}F-FDG) uptake tumor tissues in the DEN- or HBx-Tg model mice. DEN_high and low are the high and low uptake of ^{18}F-FDG in the DEN model, respectively; HBx_high and low are the high and low uptake of ^{18}F-FDG in HBx-Tg model, respectively.

Table I. Summary of HCC models by immunohistochemical analysis.

Models	^{18}F-FDG uptake[a]	Tumor type	Differentiation-grade	HK2	Glut1
DEN	High	HCA	-[b]	+++	+
	Low	Not yet cancer status	-[b]	++	+
HBx-Tg	High	HCC	Poor	+++	+
	Low	HCC	Well	+	+

[a]The ^{18}F-FDG uptake was contingent on PET/CT imaging; [b]differentiation-grade was not classified. HCA, hepatocellular adenoma; HCC, hepatocellular carcinoma; HK2, hexokinase 2; Glut1, glucose transporter 1.

from low ^{18}F-FDG uptake was well-differentiated. To determine the level of Glut1 and HK2 protein expression, IHC was performed using high and low ^{18}F-FDG uptake tumors. A stronger expression of HK2 protein was noted in tumors with high ^{18}F-FDG uptake, as compared with that in tumors with low ^{18}F-FDG uptake (Fig. 4), in the DEN and HBx-Tg models. On the other hand, comparable expression levels of Glut1 were observed in the two types of tumors (Table I and Fig. 4).

Discussion

Molecular imaging methods such as MRI, PET or optical imaging may be applicable for the non-invasive detection of induced tumors and monitoring of therapeutic effects. Early diagnosis using imaging methods also provides information associated with the mechanism of tumor development and progression and may be used for monitoring the tumors developed in internal organs, including the liver, colon or brain, as well as metastatic tumors (23,27).

Schmid *et al* (28) previously reported on the growth kinetics of DEN-induced liver tumors in mice analyzed using 7-T MRI without contrast agent. They identified that ^{18}F-FDG PET is not suitable for detection of liver tumors because of the non-specific signals obtained from highly perfused livers. However, ^{18}F-FDG PET/CT imaging was previously successfully applied in the study of liver tumors in a *c-myc* transgenic

murine model to monitor the effects of DEN as an enhancer of tumor growth and metastatic spread (29). Recently, Heijink *et al* (30) investigated the use of ^{18}F-FDG PET for the longitudinal monitoring of *Apc* mutant mice that had developed multiple colorectal adenomas. Authors of that study were able to detect abdominal hot spots reflecting metabolically active intestinal adenomas with diameters <2 mm.

In the present study, we induced HCC in mice by DEN treatment or by transgenic expression of the HBx oncoprotein. We determined the location, boundary, number and size of multiple tumor nodules using a 3-T clinical MRI unit and ^{18}F-FDG small animal PET/CT imaging. Our data demonstrated that multimodal imaging techniques can be successfully applied to evaluate and monitor tumor progression and that ^{18}F-FDG PET allows longitudinal monitoring of tumor development.

Lee *et al* (31) previously applied functional genomics to identify a best-fit murine model of human HCC from seven mouse models, including two chemically induced, four transgenic and one knockout model. Those authors concluded that the gene expression patterns of HCC induced in *c-myc*- and transforming growth factor-α-overexpressing transgenic mice and DEN-treated mice were similar to those of HCC in humans with poor prognosis. Thus, the present study made use of mouse models of HCC that mimic human HCC. Moreover, HCCs induced in an HBx-Tg mouse model were analogous to human HCCs with respect to histological findings (17).

DEN induces liver (19), gastrointestinal (32) and hematopoietic tumors (33) by alkylation of genomic DNA (23) and generation of reactive oxygen species (24). Since HCCs induced by DEN express α-fetoprotein (AFP), transgenic mice-expressing reporter genes such as luciferase or HSV1-thymidine kinase under the control of the AFP enhancer/promoter have previously been applied in the study of DEN-induced hepatocarcinogenesis (34,35). Kim *et al* (36) detected DEN-induced AFP-positive HCC using systemic administration of a recombinant adenovirus-expressing luciferase controlled by the AFP promoter/enhancer.

HBV virus is a small hepatotropic DNA virus and its carcinogenic effects on the liver are attributed to the non-structural X protein (37) that functions as a transcriptional activator of proteins, triggering signaling cascades required for hepatocyte proliferation. Moreover, the transgenic expression of HBx has been reported to induce liver cancer in mice (17) and to promote DEN-mediated hepatocarcinogenesis caused by the proliferation of altered hepatocytes (38). The present study is the first, to the best of our knowledge, to characterize HBx-induced HCC using MRI and ^{18}F-FDG PET/CT, although HCCs induced by the expression of a *c-myc* transgene in mice have also been characterized using ^{18}F-FDG PET/CT or MRI (29,39). Yu *et al* (17) reported that grossly defined HCC was observed from the age of 11-18 months by histologic investigation after sacrifice of HBx-Tg mice. However, we readily and non-invasively detected HBx gene expression-induced HCC by ^{18}F-FDG PET from the age of 11 months (Fig. 1 and 2B). We have also demonstrated a correlation between tumor sizes measured by MRI and SUV_{max} of ^{18}F-FDG PET/CT in chemical- and oncogene-induced HCC models.

In humans, detection of HCC using ^{18}F-FDG PET varies depending on the histological differentiation grade. Poorly differentiated HCC, which is associated with poorer survival, exhibited a higher uptake of ^{18}F-FDG than low-grade HCC, which is associated with a higher expression of HK2 (10,11,40). In the present study, the differentiation grade of HCC in the HBx-Tg model as determined using H&E staining was shown for the first time shown to correlate with ^{18}F-FDG uptake (Table I).

The present findings indicate the potential of non-invasive multimodal imaging to study the pathogenesis of HCC and develop highly sensitive and specific diagnostic techniques. The animal models described in this study should also yield key insights into the molecular basis of HCC and improve diagnosis and therapy.

Acknowledgements

This study was supported by a Korea Science and Engineering Foundation (KOSEF) grant funded by the Korean government (MEST) (NRF-2012M2A2A7013480). The authors would like to thank Kyungho Min for assistance with histological analysis.

References

1. Weissleder R: Scaling down imaging: Molecular mapping of cancer in mice. Nat Rev Cancer 2: 11-18, 2002.
2. Kang JH and Chung JK: Molecular-genetic imaging based on reporter gene expression. J Nucl Med 49: 164-179, 2008.
3. Kelloff GJ, Hoffman JM, Johnson B, *et al*: Progress and promise of FDG-PET imaging for cancer patient management and oncolytic drug development. Clin Cancer Res 11: 2785-2808, 2005.
4. Warburg O: On the origin of cancer cells. Science 123: 309-314, 1956.
5. Southworth R, Parry CR, Parkes HG, Medina RA and Garlick PB: Tissue-specific differences in 2-fluoro-2-deoxyglucose metabolism beyond FDG-6-P: a 19F NMR spectroscopy study in the rat. NMR Biomed 16: 494-502, 2003.
6. Okazumi S, Isono K, Enomoto K, *et al*: Evaluation of liver tumours using fluorine-18-fluorodeoxyglucose PET: characterization of tumor and assessment of effect of treatment. J Nucl Med 33: 333-339, 1992.
7. Khandani AH and Wahl RL: Applications of PET in liver imaging. Radiol Clin North Am 43: 849-860, 2005.
8. Trojan J, Schroeder O, Raedle J, *et al*: Fluorine-18 FDG positron emission tomography for imaging of hepatocellular carcinoma. Am J Gastroenterol 94: 3314-3319, 1999.
9. Delbeke D, Martin WH, Sandler MP, Chapman WC, Wright JK Jr and Pinson CW: Evaluation of benign vs malignant hepatic lesions with positron emission tomography. Arch Surg 133: 510-515, 1998.
10. Khan MA, Combs CS, Brunt EM, *et al*: Positron emission tomography scanning in the evaluation of hepatocellular carcinoma. J Hepatol 32: 792-797, 2000.
11. Kudo M: Diagnostic imaging of hepatocellular carcinoma: Recent Progress. Oncology 81: 73-85, 2011.
12. Paradis V: Histopathology of hepatocellular carcinoma. Recent Results Cancer Res 190: 21-32, 2013.
13. Kelland LR: Of mice and men: values and liabilities of the athymic nude mouse model in anticancer drug development. Eur J Cancer 40: 827-836, 2004.
14. Frese KK and Tuveson DA: Maximizing mouse cancer models. Nat Rev Cancer 7: 645-658, 2007.
15. Thorgeirsson SS and Santoni-Rugiu E: Transgenic mouse models in carcinogenesis: interaction of c-myc with transforming growth factor alpha and hepatocyte growth factor in hepatocarcinogenesis. Br J Clin Pharmacol 42: 43-52, 1996.
16. Harada N, Oshima H, Katoh M, Tamai Y, Oshima M and Taketo MM: Hepatocarcinogenesis in mice with beta-catenin and Ha-Ras gene mutations. Cancer Res 64: 48-54, 2004.
17. Yu DY, Moon HB, Son JK, *et al*: Incidence of hepatocellular carcinoma in transgenic mice expressing the hepatitis B virus X-protein. J Hepatol 31: 123-132, 1999.

18. Zheng Y, Chen WL, Louie SG, Yen TS and Ou JH: Hepatitis B virus promotes hepatocarcinogenesis in transgenic mice. Hepatology 45: 16-21, 2007.
19. Finnberg N, Stenius U and Högberg J: Heterozygous p53-deficient (+/-) mice develop fewer p53-negative preneoplastic focal liver lesions in response to treatment with diethylnitrosamine than do wild-type (+/+) mice. Cancer Lett 207: 149-155, 2004.
20. McGlynn KA, Hunter K, LeVoyer T, *et al*: Susceptibility to aflatoxin B-1-related primary hepatocellular carcinoma in mice and humans. Cancer Res 63: 4594-4601, 2003.
21. Salguero Palacios R, Roderfeld M, Hemmann S, *et al*: Activation of hepatic stellate cells is associated with cytokine expression in thioacetamide-induced hepatic fibrosis in mice. Lab Invest 88: 1192-1203, 2008.
22. Weisburger EK: Carcinogenicity studies on halogenated hydrocarbons. Environ Health Perspect 21: 7-16, 1977.
23. Teoh NC, Dan YY, Swisshelm K, *et al*: Defective DNA strand break repair causes chromosomal instability and accelerates liver carcinogenesis in mice. Hepatology 47: 2078-2088, 2008.
24. Qi Y, Chen X, Chan CY, *et al*: Two-dimensional differential gel electrophoresis/analysis of diethylnitrosamine induced rat hepatocellular carcinoma. Int J Cancer 122: 2682-2688, 2008.
25. Rao KV and Vesselinovitch SD: Age- and sex-associated diethylnitrosamine dealkylation activity of the mouse liver and hepatocarcinogenesis. Cancer Res 33: 1625-1627, 1973.
26. Naugler WE, Sakurai T, Kim S, *et al*: Gender disparity in liver cancer due to sex differences in myd88-dependent IL-6 production. Science 317: 121-124, 2007.
27. Sell S: Mouse models to study the interaction of risk factors for human liver cancer. Cancer Res 63: 7553-7562, 2003.
28. Schmid A, Rignall B, Pichler BJ and Schwarz M: Quantitative analysis of the growth kinetics of chemically induced mouse liver tumors by magnetic resonance imaging. Toxicol Sci 126:52-59, 2012.
29. Hueper K, Elalfy M, Laenger F, *et al*: PET/CT imaging of c-myc transgenic mice identifies the genotoxic n-nitroso-diethylamine as carcinogen in a short-term cancer bioassay. PLoS One 7: e30432, 2012.
30. Heijink DM, Kleibeuker JH, Nagengast WB, *et al*: Total abdominal ^{18}F-FDG uptake reflects intestinal adenoma burden in Apc mutant mice. J Nucl Med 52: 431-436, 2011.
31. Lee JS, Chu IS, Mikaelyan A, *et al*: Application of comparative functional genomics to identify best-fit mouse models to study human cancer. Nat Genet 36: 1306-1311, 2004.
32. Binato M, Kruel Schmidt M, Silveira Volkweis B, *et al*: Mouse model of diethylnitrosamine-induced gastric cancer. J Surg Res 148: 152-157, 2008.
33. Gray R, Peto R, Brantom P and Grasso P: Chronic nitrosamine ingestion in 1040 rodents: the effect of the choice of nitrosamine, the species studied and the age of starting exposure. Cancer Res 51: 6470-6491, 1991.
34. Lu X, Guo H, Molter J, *et al*: Alpha-fetoprotein-thymidine kinase-luciferase knock-in mice: a novel model for dual modality longitudinal imaging of tumorigenesis in liver. J Hepatol 55: 96-102, 2011.
35. Park JH, Kim KI, Lee YJ, *et al*: Non-invasive monitoring of hepatocellular carcinoma in transgenic mouse with bioluminescent imaging. Cancer Lett 310: 53-60, 2011.
36. Kim KI, Park JH, Lee YJ, *et al*: In vivo bioluminescent imaging of α-fetoprotein-producing hepatocellular carcinoma in the diethylnitrosamine-treated mouse using recombinant adenoviral vector. J Gene Med 14: 513-520, 2012.
37. Koike K: Hepatitis B virus X gene is implicated in liver carcinogenesis. Cancer Lett 286: 60-68, 2009.
38. Madden CR, Finegold MJ and Slagle BL: Hepatitis B virus X protein acts as a tumor promoter in development of diethylnitrosamine-induced preneoplastic lesions. J Virol 75: 3851-3858, 2001.
39. Freimuth J, Gassler N, Moro N, *et al*: Application of magnetic resonance imaging in transgenic and chemical mouse models of hepatocellular carcinoma. Mol Cancer 9: 94, 2010.
40. Lee JD, Yang WI, Park YN, *et al*: Different glucose uptake and glycolytic mechanisms between hepatocellular carcinoma and intrahepatic mass-forming cholangiocarcinoma with increased (18)F-FDG uptake. J Nucl Med 46: 1753-1759, 2005.